Correlation between quarter-point angle and nuclear radius *

Wei-Hu Ma(马维虎) [1,2,3;1)] Jian-Song Wang(王建松)[1;2)] S. Mukherjee[4]
Qi Wang(王琦)[1] D. Patel[1] Yan-Yun Yang(杨彦云)[1] Jun-Bing Ma(马军兵)[1]
Peng Ma(马朋)[1] Shi-Lun Jin(金仕伦)[1] Zhen Bai(白真)[1] Xing-Quan Liu(刘星泉)[1]

[1] Institute of Modern Physics, Chinese Academy of Science, Lanzhou 730000, China
[2] University of Chinese Academy of Science, Beijing 100049, China
[3] Lanzhou University, Lanzhou 730000, China
[4] Physics Department, Faculty of Science, M.S. University of Baroda, Vadodara - 390002, India

Abstract: The correlation between quarter-point angle of elastic scattering and nuclear matter radius is studied systematically. Various phenomenological formulae with parameters for nuclear radius are adopted and compared by fitting the experimental data of quarter point angle extracted from nuclear elastic scattering reaction systems. A parameterized formula related to binding energy is recommended, which gives a good reproduction of nuclear matter radii of halo nuclei. It indicates that the quarter-point angle of elastic scattering is quite sensitive to the nuclear matter radius and can be used to extract the nuclear matter radius.

Keywords: nuclear radius, quarter point angle, nuclear elastic scattering reaction

PACS: 21,10,Dr **DOI:** 10.1088/1674-1137/41/4/044103

1 Introduction

In recent years, nuclear reactions with unstable or weakly bound nuclei that have low breakup threshold and exotic structure have shown remarkable features which are different from those of tightly bound nuclei. It is interesting to understand and revisit in detail the difference in the reaction mechanisms using tightly bound, weakly bound, unbound and halo nuclei. They are defined and differentiated by a combination of binding energy and separation energy. The tightly bound nuclei are even-even nuclei with high binding energy per nucleon. Halo nuclei (like typical halo nuclei ^{6}He, ^{11}Li and ^{11}Be) have very low binding energy per nucleon and very low separation energy of the outermost nucleons. The binding energy per nucleon of weakly bound nuclei are in between those of tightly bound nuclei and halo nuclei. Very recently, a phenomenological comparison of reduced reaction cross sections of different reaction systems was proposed by using Wong's model [1–3]. Several authors have extracted the quarter-point angle from the elastic scattering angular distribution reaction cross section, in order to compare weakly and tightly bound projectiles [4–6]. The quarter point angle, which is also called the "grazing angle" or "rainbow angle", is one of the most conspicuous features of heavy-ion elastic scattering at above-barrier energies. Accordingly, the radius of interaction $R_{\rm int}$, correlating with quarter-point angle, is the sum of projectile and target radius and approximately equals the classical apsidal distance, the distance of closest approach, evaluated at the energy for which the experimental cross section is one-quarter of the corresponding Rutherford cross section [7]. Earlier evaluations of $R_{\rm int}$ were given by $r_0(A_{\rm p}^{1/3}+A_{\rm t}^{1/3})$, where $A_{\rm p}$ and $A_{\rm t}$ are the mass numbers of projectile and target, respectively. It has been found that values of r_0 ranging from 1.20 to 1.30 fm are the most appropriate values for heavy ion interactions at energies $\geqslant$ 10.0 MeV/u ([8] and references therein).

Experimentally, the nuclear radius (or nuclear matter distribution) can be determined by the measurement of electron scattering, isotope shift and interaction cross section etc. Since the electron is structureless and the electromagnetic interaction is very well known, the charge distribution of a nucleus can be precisely obtained from the electron scattering measurements. The proton distribution can be deduced from the nuclear charge distribution in the case of stable nuclei. However, for un-

Received 18 October 2016, Revised 29 November 2016

∗ Supported by National Natural Science Foundation of China (U1432247, 11575256), National Basic Research Program of China (973 Program)(2014CB845405 and 2013CB83440x) and (SM) Chinese Academy of Sciences President's International Fellowship Initiative (2015-FX-04)

1) E-mail: weihuma@impcas.ac.cn

2) E-mail: jswang@impcas.ac.cn

stable nuclei, being short-lived and difficult to use as a target, especially halo nuclei, one usually uses the isotope method or interaction cross section measurements to determine the size of the nucleus. To be more precise, electron scattering is better than isotope shift and isotope shift is better than interaction cross section. Moreover, the interaction cross section is highly model dependent. Earlier, it was observed that the nuclear size is obviously correlated to the quarter-point angle. This is because the quarter-point angle is a function of $R_{\rm int}$. This indicates that we may extract the radius of unstable nuclei from the experimental quarter-point angle. This could be a new experimental method to determine the nuclear size.

As introduced above, interaction radius can be extracted from the quarter-point angle through the elastic scattering angular distribution of the reacting system. Based on the concept of quarter-point angle, the main objective of this work is to compare tightly bound, weakly bound (stable) and halo projectiles using the phenomenological formula for interaction radius. This difference in the three kinds of projectiles can be employed to find a better understanding of interaction radius. Furthermore, nuclear radius can also be obtained from this analysis.

2 Phenomenological formulae with parameters for radius of interaction

The theoretical quarter-point angle as a function of the dimensionless variable x was described in Ref. [6].

$$\theta_{1/4} = 2\arcsin[1/(2x-1)], \tag{1}$$

where $x = E_{\rm cm}/V_{\rm coul}$, the ratio of the center of mass energy $E_{\rm cm}$ to Coulomb barrier $V_{\rm coul}$. The experimental values of the quarter-point angle were extracted from the available experimental data of the elastic scattering by fitting the angular distribution of the differential cross sections with the optical model. The corresponding center-of-mass energies can also be obtained from experiments. The Coulomb barrier was determined by $Z_{\rm p}Z_{\rm t}e^2/R_{\rm int}$, where $Z_{\rm p}$ and $Z_{\rm t}$ are the number of protons in the projectile and target respectively. In addition, the value of $R_{\rm int}$ can be obtained from the experimental values of quarter-point angle by the following relationship: $\frac{Z_{\rm p}Z_{\rm t}e^2}{2E_{\rm cm}}\cdot\left(1+\frac{\csc(\theta_{1/4})}{2}\right)\Big)$. The experimental values of quarter point angle are given in Appendix A.

The introduction of the reduced energy parameter x is very useful to compare the quarter-point angle of different reaction systems together in one graph. Figure 1 shows the comparison of quarter point angles obtained from a large amount of experimental data, using different tightness of projectiles, i.e., tightly bound, weakly bound, and halo projectiles. In general, the experimental values of quarter point angle of these three different type of projectiles successively decrease when the value of x is fixed. However, all the experimental points of quarter-point angle are obviously lower than the curve of the theoretical quarter-point angle function (TQAF, the formular (1)). This is because the theoretical $R_{\rm int}$ is simply given by the phenomenological formula $A_{\rm p}^{1/3}$+$A_{\rm t}^{1/3}$ (PF1, as employed by L. Jin et al. [6]) to calculate the value of x.

Additionally, from Fig. 1, the comparison of the three kinds of projectiles is less distinguishable when a large amount of experimental data is taken into account, although the values of the quarter point angle follow a successively decreasing general trend from the tightly bound to the halo for a fixed value of x. In general, for tightly bound systems with x varying from 0.8 to 2.0, experimental points exhibit an increasing deviation from the curve with increasing x. This anomaly was observed while deriving $R_{\rm int}$ by using the usual formula $(A_{\rm p}^{1/3}+A_{\rm t}^{1/3})$. A similar wide distribution can also be observed in the case of weakly bound and halo systems.

According to the above discussion, it is necessary to introduce a modified formula for $R_{\rm int}$ as given by $a\cdot A_{\rm p}^{1/3}+b\cdot A_{\rm t}^{1/3}$ (PF2), where the parameters a and b are fitted by extracting experimental $R_{\rm int}$ separately for tightly bound, weakly bound and halo projectiles.

In the fitted values, as shown in Table 1, the parameter b (b=1) is kept constant for the all three kinds of system, assuming the target to be stable. The fitted parameter a increases from tightly bound to halo projectiles. It can be distinctly observed that the fitted values of parameter a for tightly bound, weakly bound and halo projectiles describe the difference between the reaction systems and well indicate the size of projectiles from the expression $a\cdot A_{\rm p}^{1/3}$. This is in accordance with the nuclear size obtained from previous studies. This also clearly indicates that the radius calculated by the expression $A_{\rm p}^{1/3}+A_{\rm t}^{1/3}$ in order to compare the different kinds of projectiles results in the underestimation of the size of weakly bound projectiles, and even more in the case of halo projectiles.

Table 1. The fitted values of a and b for tightly bound, weakly bound and halo projectiles.

projectile	a/fm	b/fm
tightly bound	1.123	1.00
weakly bound	1.187	1.00
halo	1.333	1.00

Thus the modified expression of $R_{\rm int}$ can reduce the deviation between the experimental data and the theoretical curve of the quarter-point angle as a function of x. In Fig. 2 , the result of the modification is shown.

When compared with the points in Fig. 1, the deviation between the experimental data and the theoretical curve and among the three kinds of projectiles is diminished.

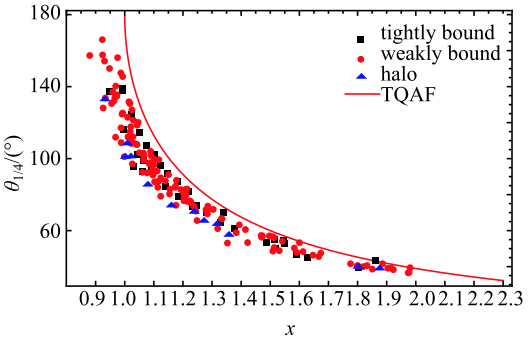

Fig. 1. (color online) The quarter point angle as a function of reduced energy x in the interval from 0.8 to 2.0 for the phenomenological formula $R_{\rm int}=A_{\rm p}^{1/3}+A_{\rm t}^{1/3}$ (PF1). The color points stand for the experimental quarter-point angles. The theoretical quarter-point angle function is labeled as TQAF.

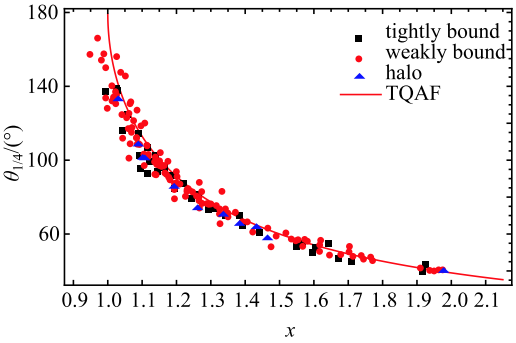

Fig. 2. (color online) Same as Fig. 1, except for phenomenological formula (PF2).

With the enlightenment of reducing the difference in the quarter point angle values among the three kinds of projectiles by using modified $R_{\rm int}$, it is feasible to find a better phenomenological formula to give a better description of the strong absorption radius. To begin with, the nuclear radius based on the liquid drop model was used. Additionally, nucleon distribution having finite surface thickness was assumed instead of uniform distribution. Considering the isospin symmetry that distinguishes between proton and neutron, affected equally by the nuclear strong force, the improved expression of $R_{\rm int}$ with parameters r_0, r_1, r_2 and a_z is given by (PF3) [9],

$$R_{\rm int}=\sum_{\rm i=p,t}R_{\rm i}; \tag{2}$$

$$R_{\rm i}=\left(\left(r_0+\frac{r_1}{A_{\rm i}^{2/3}}+\frac{r_2}{A_{\rm i}^{4/3}}\right)+a_z\frac{Z_{\rm i}-Z_{\rm stable}}{A_{\rm i}}\right)A_{\rm i}^{1/3}; \tag{3}$$

where $Z_{\rm stable}=\dfrac{A_i}{1.98+0.016\cdot A_{\rm i}^{2/3}}$; i denotes projectile and target. The values of the parameters r_0, r_1, r_2 and a_z obtained by fitting the experimental data, were 1.0152 fm, 0.6383 fm, −1.2781 fm and −0.2981 fm respectively. However, as shown in Fig. 3 (a), the quarter point angle values are still inconsistent with respect to the three types of projectile, although the deviation between the experimental data and the theoretical curve decreases. Thus the modified formula given by PF3 is not adequate to accurately describe the nuclear size, especially for the halo nuclei. In order to obtain a consistent description for nuclear size, it is important to discuss this phenomenological formulation with further improvement by considering the binding energy of the nuclei. According to quantum mechanics, the nuclear rms radius is inversely proportional to the binding energy. The relation between the rms radii and the binding energy can be obtained from the simplified N single-particle Schrödinger equation as, $R(B)=\dfrac{4.04}{\sqrt{B(A)}}$[10]. However, this relation is not sufficient for good agreement with the experimental data. A modified quantitative formula of the nuclear rms radius as a function of binding energy per nucleon was introduced and discussed by Wang et al. [11]. It is important to take into account the binding energies and based on this fact, the theoretical $R_{\rm int}$ is given by (PF4)

$$R_{\rm int}=\sum_{\rm i=p,t}R_{\rm i}; \tag{4}$$

$$R_{\rm i}=\lambda_0A_{\rm i}^{1/3}+\lambda_1+\lambda_2\frac{I_{\rm i}}{\sqrt{B_{\rm i}}}+\left(\lambda_3\frac{I_{\rm i}}{\sqrt{B_{\rm i}}}\right)^2; \tag{5}$$

where $I_{\rm i}=\dfrac{A_{\rm i}-2Z_{\rm i}}{A_{\rm i}}$, denotes the symmetry parameter, $B_{\rm i}$ is the binding energy per nucleon, and subscripts denotes projectile and target. The experimental data of quarter-point angle were fitted to obtain the parameters λ_0=0.9776 fm, λ_1=0.2475 fm, $\lambda_2=-0.1492$ fm/MeV$^{1/2}$ and λ_3=10.7186 fm/MeV. The experimental values of binding energy were taken from the literature [12] and were used to determine $B_{\rm i}$. As a result, the deviation between the experimental and the theoretical curve for all three types of projectile (mainly between the tightly bound and the halo) were diminished as can be seen in Fig. 3(b).

The goodness of fit for PFs was obtained by the standard deviation of the dependent variable S ($S=\sqrt{SUM((y_{\rm i}-f(x_{\rm i}))^2)/N}$, where N is the number of degrees of freedom). This is a number that indicates how well data fit a curve, with a lower S indicating a better fit. The S values for the four PFs (PF1, PF2, PF3 and PF4) are 0.4676, 1.0612, 0.2608 and 0.2564 respectively,

and the differences among the goodness of the fits are obvious. The binding energy dependent formula PF4 can be considered the best formula in the present work and is recommended. Using the results from the above method and comparing them with the fitted data as shown in Figs. 1–3, one can emphasize the importance of the binding energy to understand the nuclear size, especially in the case of halo nuclei. For a clear justification, the next section gives a more detailed comparison.

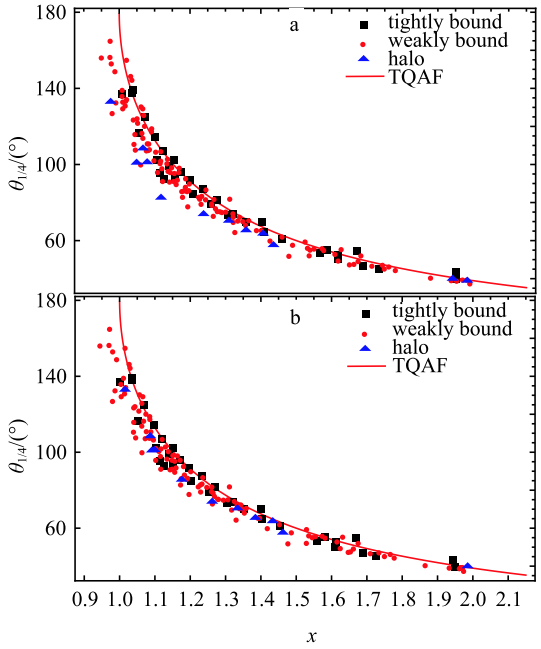

Fig. 3. (color online) Theoretical and experimental quarter point angle values for three types of projectiles using PF3 (a) and PF4 (b). The color points are for the experimental quarter-point angle values. The experimental data were used in the interval of x from 0.8 to 2.0. The theoretical quarter-point angle function is labeled as TQAF.

3 Comparison of the four phenomenological formulae

In this section, we give a quantitative comparison of the four phenomenological formulae (PF1 to PF4). We define a goodness of fit ratio $\eta = \dfrac{x - x_{\rm PF}}{x_{\rm PF}}$ that will estimate the deviation between the experimental quarter-point angle and the theoretical curve (TQAF). In other words, the smaller the value of η, the less the deviation. In this relation $x_{\rm PF}$ is determined by the center-mass energy and the Coulomb barrier via the phenomenological formulae, $x_{\rm PF} = E_{\rm cm}/V_{\rm coul}$. However, x is directly calculated by using Eq. (1), namely, using the TQAF curve. Both $x_{\rm PF}$ and x correspond to the same quarter-point angle extracted from elastic scattering angular distribution of the reacting systems. The comparison of η in terms of the four phenomenological formulae (PF1 to PF4) is shown in Fig. 4. It is clear from the figure that the modified formulae PF2, PF3 and PF4 show a better agreement as compared to PF1 so far as the deviation between the experimental data and the theoretical curve (TQAF) is concerned. The advantages and disadvantages of the four methods for calculating $R_{\rm int}$ are more clearly understood when comparing the deviation between tightly bound and halo projectiles.

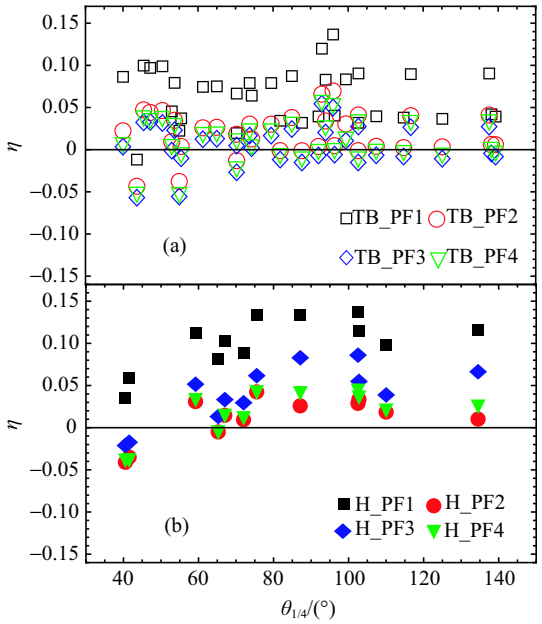

Fig. 4. (color online) Comparison of the four phenomenological formulae with the experimental data used in the interval of x from 0.8 to 2.0. The open symbols for tightly bound nuclei are shown in (a) and the solid symbols for the halo nuclei are shown in (b).

This deviation between tightly bound and halo projectiles by the four methods may be more clearly obtained by introducing another parameter $\Delta\eta = \overline{\eta_{\rm H}} - \overline{\eta_{\rm TB}}$, where $\overline{\eta_{\rm H}}$ is the arithmetic mean of η for halo nuclei and $\overline{\eta_{\rm TB}}$ is that for tightly bound nuclei. In addition, the inconsistency of the experimental points can be found for tightly bound systems with two clear groups (taking Fig. 5 as a sample case) while for the weakly bound systems there is a scattered distribution. In Fig. 5, the large η values for the sets of experimental quarter-point angle points of the tight bound nuclei far from the curve of TQAF are mainly extracted from the elastic scattering reaction systems of ^{16}O+^{40}Ca, ^{16}O+^{42}Ca, ^{16}O+^{56}Fe, and ^{16}O+^{90}Zr, of which the incident energies are in the range 28–68 MeV. The smaller values for the points near the TQAF curve are mainly extracted from the elastic scattering reaction systems of ^{16}O+^{208}Pb and ^{12}O+^{208}Pb, of which the incident energies are in the range 44–140

MeV. We take the case of tightly bound nuclei to explain this feature. Analogically, the exact deviation between $\overline{\eta_{1-\mathrm{TB}}}$ and $\overline{\eta_{2-\mathrm{TB}}}$ is given by $\Delta\eta_{\mathrm{TB}} = \overline{\eta_{1-\mathrm{TB}}} - \overline{\eta_{2-\mathrm{TB}}}$, where $\overline{\eta_{1-\mathrm{TB}}}$ is the arithmetic mean of the group of experimental quarter-point angle points of tight bound nuclei far from the TQAF curve and $\overline{\eta_{2-\mathrm{TB}}}$ is that near the TQAF curve. $\Delta\eta$ denotes the difference between tightly bound and halo nuclei, and $\Delta\eta_{\mathrm{TB}}$ reflects the difference of the two groups of nuclei in the tightly bound case. The calculated values of $\Delta\eta$ and $\Delta\eta_{\mathrm{TB}}$ are shown in Table 2. From these values, the results given by PF4 show the minimum values for both $\Delta\eta$ and $\Delta\eta_{TB}$. Therefore, one can conclude that among all the four phenomenological formulae, PF4 shows the best improvement in the present work for all the three types of nuclei. Thus in the present work, PF4 is recommended for giving better consistency among tightly bound systems, besides reducing the deviation between the experimental data and the theoretical curve of quarter-point angle.

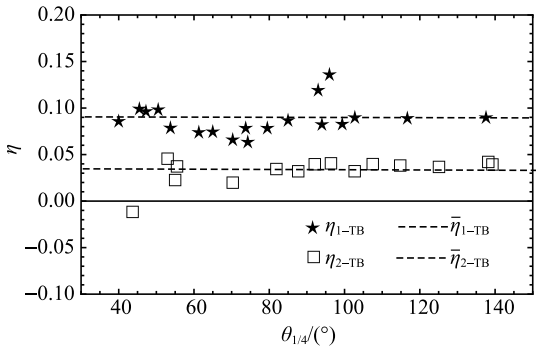

Fig. 5. (color online) Comparison of η with the experimental data used in the interval of x from 0.8 to 2.0 for the sets of experimental quarter-point angle points of the tight bound nuclei near and far from the TQAF curve for PF1. $\eta_{1-\mathrm{TB}}$ is the points of η far from the TQAF curve and $\eta_{2-\mathrm{TB}}$ is the points of η near the TQAF curve.

Table 2. The values of $\Delta\eta$ and $\Delta\eta_{\mathrm{TB}}$ for PF1, PF2, PF3 and PF4.

	PF1	PF2	PF3	PF4
$\Delta\eta$	0.0374	0.0077	0.0342	0.0059
$\Delta\eta_{\mathrm{TB}}$	0.056	0.040	0.039	0.033

In conclusion, the theoretical radius of interaction given by PF1 is not a good formula, although it can be used to compare the different tightness of systems. PF2, with parameters separately fitted by tightly bound, weakly bound and halo projectiles, is a parameterized method to do the comparison. For finding a unified formula for nuclear radius, namely for the radius of interaction, PF3 and PF4 are compared. However, the improvement in PF3 with symmetry dependence considered is not good enough to consistently describe the nuclear size. Finally, PF4 with the binding energy considered is recommended by this work for a phenomenological formula for R_{int}, as it reduces the deviation not only between the experimental data and the theoretical curve but also among the three kinds of projectiles. The inconsistency among the tightly bound systems is also improved by PF4.

4 Calculation of nuclear radius

As discussed above, PF4 not only reduces the deviation between the experimental data and the theoretical curve but also among the three kinds of projectiles, when we compare the four parameterized theoretical formulae (PF1 to PF4) in order to obtain the radius of interaction R_{int}. This means that if we use the recommended formula PF4 for calculating R_{int} of systems with tightly bound, weakly bound and halo projectiles to calculate x, and plot $\theta_{1/4}$ vs x, we can see that all the systems are on one curve of TQAF. The nuclear size is obviously correlated to the quarter-point angle, because x is a function of R_{int}, which indicates that we may extract the radius of nuclei from the experimental quarter-point angle.

For all applications, we calculate the radius of nuclei as projectiles using the formulae fitted from experimental quarter-point angle and separately compare them with the experimental charge radius [13] for tightly-bound (Fig. 6) and weakly-bound nuclei (Fig. 7) and with experimental root mean square (rms) matter radius (Table 3) for halo nuclei (Fig. 8). For light nuclei, the nuclear experimental charge radius usually agrees with the mass radius, but for heavy nuclei, which have more neutrons than protons, the mass radius might be larger than the charge radius. For halo nuclei, the charge radius does not usually reflect their size, but R_{rms} can do so. In the present work, to compare with the calculated

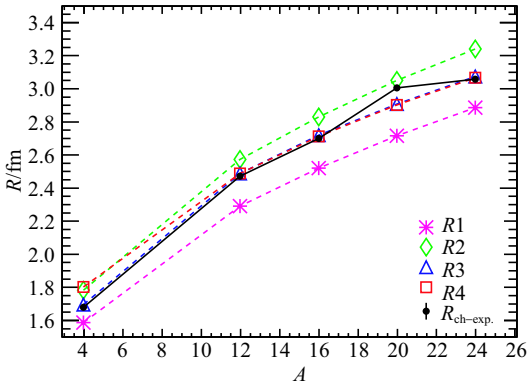

Fig. 6. (color online) Comparison of the calculated mass radius ($R1$, $R2$, $R3$ and $R4$) based on the four phenomenological formulae with nuclear charge radius for tightly-bound nuclei ^{4}He, ^{12}C, ^{16}O, ^{20}Ne and ^{24}Mg.

radii $R_{\rm int}$ extracted from the quarter point angle, we take the experimental charge radius to be the size of the light tightly bound and weakly bound nuclei and use the experimental $R_{\rm rms}$ as the size of the halo nuclei. As shown in Figs. 7 and 8, the calculation of tightly-bound and light weakly-bound nuclei based on PF3 and PF4 can be deemed a better representation for determining nuclear size than PF1 and PF2. The goal of extracting the radius of exotic nuclei from the experimental quarter-point angle can be embodied by the calculation based on PF4, as shown in Fig. 8, which clearly shows the feasibility of acquiring the radius of halo nuclei via the experimental quarter-point angle. From the comparison, the calculation for light halo nuclei based on PF3 does not agree with the experimental values.

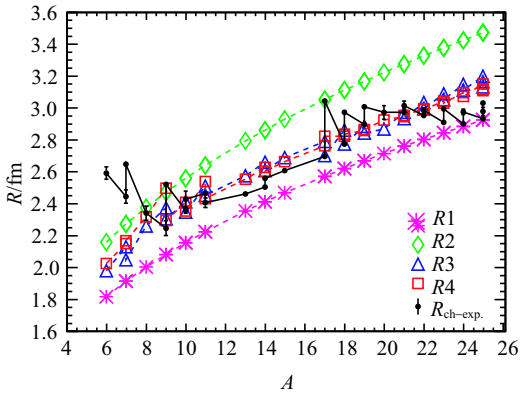

Fig. 7. (color online) Comparison of the calculated mass radius based on the four phenomenological formulae PF1 to PF4 ($R1$, $R2$, $R3$ and $R4$) with nuclear rms charge radius for weakly-bound nuclei.

Table 3. Experimental values of rms matter radii for light halo nuclei.

nuclei	$R_{\rm rms}$/fm	Ref.
^{6}He	2.30±0.07	[16]
^{8}He	2.69±0.03	[17]
^{8}B	2.38±0.04	[18]
^{9}C	2.71±0.32	[19]
^{10}Be	2.479±0.028	[20]
^{10}C	2.42±0.10	[21]
^{11}Li	$3.34^{+0.04}_{-0.08}$	[22]
^{11}Be	2.73±0.05	[23]
^{11}C	2.46±0.03	[20]
^{12}N	2.47±0.07	[24]
^{13}O	2.53±0.05	[24]
^{14}Be	3.10±0.15	[25]
^{17}B	2.99±0.09	[25]
^{17}F	2.71±0.18	[26]
^{17}Ne	2.75±0.07	[24]
^{19}B	3.11±0.13	[25]
^{23}Al	2.905±0.250	[26]
^{27}P	3.020±0.155	[26]

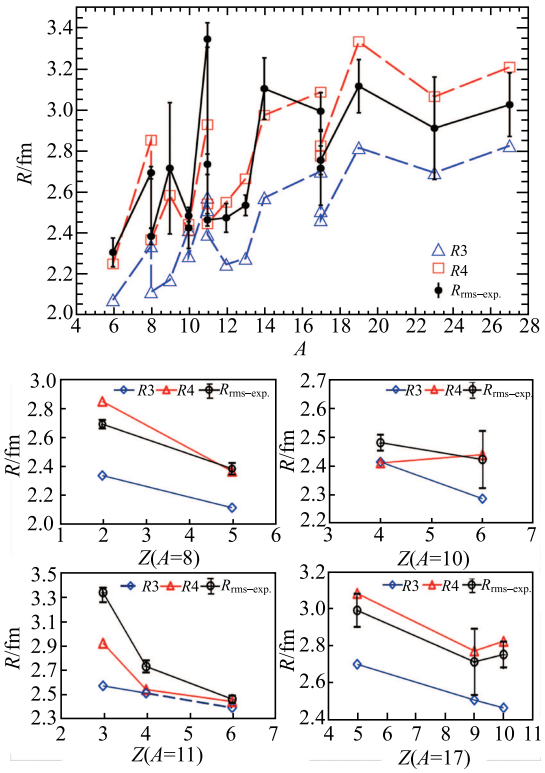

Fig. 8. (color online) Comparison of the calculated mass radius based on the phenomenological formulae PF3 and PF4 ($R3$ and $R4$) with nuclear rms matter radius for halo nuclei.

As a matter of fact, the elastic scattering of a halo nucleus from a stable target can give simple direct evidence for the structure of the halo nucleus [14]. The angular distribution of elastic scattering reactions show a maximum difference for incident energies around the top of the Coulomb barrier, thereby suggesting that it is in this energy region that the elastic scattering is most sensitive to the surface diffuseness of the nuclear structure of the exotic projectiles [15]. The quarter-point angle as a function of radius of interaction $R_{\rm int}$, obtained via angular distributions of elastic scattering cross section, is related to the actual reaction mechanisms, which is not only related to the size of the nuclei but also to the elastic scattering reactions with coupling to the channels of inelastic scattering or other reactions. The nuclear properties, such as nuclear radius, isospin symmetry and binding energy per nucleon, will affect the strength of the couplings for different incident energies. Inversely, we can extract information about the structure, such as the nuclear size, from elastic scattering reactions. Experimentally, the nuclear radius can be determined by electron scattering, isotope shift and interaction cross section etc. Since the electron is structureless and the electromagnetic interaction is known very well, the charge

distribution of nuclei can be precisely measured by electron scattering. However, it is suitable for stable nuclei only, as unstable nuclei are short-lived and difficult to use as targets. For unstable nuclei and especially for halo nuclei, the isotope method or interaction cross section are usually used to measure the size of nuclei. However, extracting the radius of unstable nuclei from the experimental quarter-point angle could be a useful tool as a new experimental measurement. Therefore, PF4 with more details of structure (spatial extension, isospin symmetry and binding energy) is recommended for the nuclear radius by this work.

5 Conclusions

The motivation of this work is to correlate quarter-point angle and nuclear radius. Theoretical radii of interaction $R_{\rm int}$ were obtained and compared. In this work, four phenomenological formulae (PF1 to PF4) were presumed and the parameters for different formulae were fitted by using the extracted experimental values of $R_{\rm int}$. Considering the different kinds of reaction systems, the four phenomenological formulae were analyzed and discussed. Based on the above mentioned formulae, the radii of different kinds of nuclei as projectiles were obtained and explained in detail. As a result, the parameterized formula related to binding energy was recommended. In conclusion, the deviation between the experimental data and the theoretical curve and among the three kinds of projectiles can be minimized by appropriately calculating the nuclear radius in order to determine the radius of interaction. This may lead to a better understanding of the nuclear structure and the actual reaction mechanisms using the three types of projectiles (strongly bound, weakly bound and halo nuclei).

Appendix A

The extracted experimental quarter-point angle data for tightly bound and halo systems are arranged in the following Table 4. This data was obtained from [http://nrv.jinr.ru/nrv/]. The data for weakly bound projectiles, ^{6}Li, ^{7}Li, ^{9}Be, ^{11}B, ^{14}N, ^{15}N and ^{19}F can be also found in [http://nrv.jinr.ru/nrv/].

Table 4. The extracted experimental quarter-point angle data for tightly bound and halo systems.

reaction systems	$E_{\rm cm}$/MeV	$\theta_{\rm cm}$/(°)	reaction systems	$E_{\rm cm}$/MeV	$\theta_{\rm cm}$/(°)
^{12}C+^{28}Si	16.80	99.4	^{12}C+^{28}Si	34.51	31.0
^{12}C+^{28}Si	45.50	24.8	^{12}C+^{28}Si	130.48	6.4
^{12}C+^{208}Pb	59.47	139.3	^{12}C+^{208}Pb	61.36	125.1
^{12}C+^{208}Pb	66.09	102.7	^{12}C+^{208}Pb	70.81	87.7
^{12}C+^{208}Pb	80.27	70.3	^{12}C+^{208}Pb	90.76	55.5
^{12}C+^{208}Pb	111.57	43.7	^{12}C+^{208}Pb	170.18	24.6
^{12}C+^{208}Pb	283.64	14.0	^{12}C+^{208}Pb	397.09	9.6
^{16}O+^{12}C	10.29	96.0	^{16}O+^{12}C	15.43	55.0
^{16}O+^{12}C	18.00	40.0	^{16}O+^{12}C	26.57	30.0
^{16}O+^{12}C	34.29	20.8	^{16}O+^{12}C	56.57	12.3
^{16}O+^{16}O	37.50	22.7	^{16}O+^{16}O	40.50	20.6
^{16}O+^{16}O	43.50	19.5	^{16}O+^{16}O	46.00	18.0
^{16}O+^{16}O	47.50	17.3	^{16}O+^{16}O	58.00	13.6
^{16}O+^{40}Ca	28.57	93.0	^{16}O+^{40}Ca	33.57	74.3
^{16}O+^{40}Ca	42.86	47.3	^{16}O+^{40}Ca	40.55	50.5
^{16}O+^{40}Ca	43.45	45.5	^{16}O+^{56}Fe	31.11	137.6
^{16}O+^{56}Fe	32.67	116.7	^{16}O+^{56}Fe	34.22	102.8
^{16}O+^{56}Fe	35.78	94.0	^{16}O+^{56}Fe	37.33	85.0
^{16}O+^{56}Fe	38.89	79.5	^{16}O+^{56}Fe	40.44	73.8
^{16}O+^{56}Fe	42.00	70.3	^{16}O+^{56}Fe	43.56	65.0
^{16}O+^{56}Fe	45.11	61.3	^{16}O+^{90}Zr	67.92	53.8
^{16}O+^{90}Zr	117.34	26.4	^{16}O+^{90}Zr	165.06	17.8
^{16}O+^{208}Pb	120.25	53.0	^{16}O+^{208}Pb	178.29	31.2

Continued

reaction systems	$E_{\rm cm}$/MeV	$\theta_{\rm cm}/(^\circ)$	reaction systems	$E_{\rm cm}$/MeV	$\theta_{\rm cm}/(^\circ)$
^{16}O+^{208}Pb	77.07	138.2	^{16}O+^{208}Pb	81.71	114.8
^{16}O+^{208}Pb	83.57	107.5	^{16}O+^{208}Pb	87.29	96.4
^{16}O+^{208}Pb	89.14	92.1	^{16}O+^{208}Pb	94.71	81.9
^{6}He+^{65}Cu	17.90	41.5	^{6}He+^{65}Cu	27.50	25.0
^{6}He+^{120}Sn	17.19	75.5	^{6}He+^{120}Sn	18.86	67.0
^{6}He+^{120}Sn	19.52	65.3	^{6}He+^{197}Au	38.82	40.5
^{6}He+^{208}Pb	21.38	110.0	^{6}He+^{208}Pb	26.24	72.0
^{6}He+^{208}Pb	28.77	59.2	^{6}He+^{208}Pb	53.46	27.8
^{6}He+^{209}Pb	21.87	102.8	^{8}B+^{58}Ni	22.23	134.5
^{8}B+^{58}Ni	23.90	102.5	^{8}B+^{58}Ni	25.75	87.1

References

1 J. J. Kolata and E. F. Aguilera, Phys. Rev. C, **79**: 027603 (2009)
2 J. M. B. Shorto et al, Phys. Lett. B, **678**: 77 (2009)
3 C. Y. Wong, Phys. Rev. Lett., **31**: 766 (1973)
4 W. E. Frahn, Phys. Rev. Lett., **26**: 568 (1971)
5 S. H. Fricke et al, Nucl. Phys. A, **500**: 399 (1989)
6 L. Jin et al, Phys. Rev. C, **86**: 057602 (2012)
7 F. I. A. de Almeida and M. S. Hussein, Phys. Rev. C, **31**: 2120 (1985)
8 E. U. Khan et al, Radiation Measurements, **34**: 227 (2001)
9 I. Angeli, INDC(HUN)-033, September 1999 (IAEA Nuclear Data Section,Vienna) https://www-nds.iaea.org/publications/indc/indc-hun-0033/
10 E. F. Helfter, M. de Llano, and I.A. Mitropolsky, Phys. Rev. C, **30**: 2042 (1984)
11 J. S. Wang et al, Nucl. Phys. A, **691**: 618-630 (2001)
12 M. Wang et al, Chinese Phys. C, **36**: 12 (2012)
13 I. Angeli and K.P. Marinova, Atomic Data and Nuclear Data Tables, **99**: 69-95 (2013)
14 R. C. Johnson et al, Phys. Rev. Letts., **79**: 2771 (1997)
15 N. Keeley et al, Progress in Particle and Nuclear Physics, **63**: 396-447 (2009)
16 G. D. Alkhazov et al, Phys. Rev. Lett., **78**: 2313 (1997)
17 I. Tanihata et al, Phys. Rev. Lett., **55**: 24 (1985)
18 I. Tanihata et al, Phys. Lett. B, **206**: 592 (1988)
19 R. E. Warner et al, Phys. Rev. C, **74**: 014605 (2006)
20 E. Liatard et al, Europhys. Lett., **13**: 401 (1990)
21 C. Jouanne et al, Phys. Rev. C, **72**: 014308 (2005)
22 T. Moriguchi et al, Phys. Rev. C, **88**: 024610 (2013)
23 A. Ozawa et al, Nucl. Phys. A, **693**: 32-62 (2001)
24 A. Ozawa et al, Nucl. Phys. A, **608**: 63 (1996)
25 T. Suzuki et al, Nucl. Phys. A, **658**: 313 (1999)
26 H. Y. Zhang et al, Nucl. Phys. A, **707**: 303 (2002)